

# Dielectric Properties of Ultrathin CaF<sub>2</sub> Ionic Crystals

Chao Wen, Alexander G. Bانشchikov, Yury Y. Illarionov, Werner Frammelsberger, Theresia Knobloch, Fei Hui, Nikolai S. Sokolov, Tibor Grasser, and Mario Lanza\*

Mechanically exfoliated 2D hexagonal boron nitride (h-BN) is currently the preferred dielectric material to interact with graphene and 2D transition metal dichalcogenides in nanoelectronic devices, as they form a clean van der Waals interface. However, h-BN has a low dielectric constant ( $\approx 3.9$ ), which in ultrascaled devices results in high leakage current and premature dielectric breakdown. Furthermore, the synthesis of h-BN using scalable methods, such as chemical vapor deposition, requires very high temperatures ( $>900$  °C), and the resulting h-BN stacks contain abundant few-atoms-wide amorphous regions that decrease its homogeneity and dielectric strength. Here it is shown that ultrathin calcium fluoride (CaF<sub>2</sub>) ionic crystals could be an excellent solution to mitigate these problems. By applying  $>3000$  ramped voltage stresses and several current maps at different locations of the samples via conductive atomic force microscopy, it is statistically demonstrated that ultrathin CaF<sub>2</sub> shows much better dielectric performance (i.e., homogeneity, leakage current, and dielectric strength) than SiO<sub>2</sub>, TiO<sub>2</sub>, and h-BN. The main reason behind this behavior is that the cubic crystalline structure of CaF<sub>2</sub> is continuous and free of defects over large regions, which prevents the formation of electrically weak spots.

The integration of 2D materials in solid-state electronic devices and circuits may allow developing advanced applications with superior performance. However, the interaction of 2D materials like graphene and 2D transition-metal dichalcogenides (TMDs) with adjacent 3D dielectrics in electronic devices (normally SiO<sub>2</sub> or metal oxides) has been shown to be very problematic, as the 2D/3D interface usually contains a large

number of defective bonds.<sup>[1]</sup> This promotes uncontrollable charge trapping and de-trapping, which creates unwanted deviations of several parameters of the devices (i.e., hysteresis and threshold voltage in transistors), and results in a faster device degradation.<sup>[2]</sup> To solve this problem, one common strategy is to use multilayer hexagonal boron nitride (h-BN) as substrate and/or dielectric.<sup>[3,4]</sup> However, so far h-BN dielectrics only work reliably when synthesized by (non-scalable) mechanical exfoliation, which results in a considerably lower amount of defects.<sup>[4]</sup> When the h-BN is synthesized using scalable methods, such as chemical vapor deposition (CVD), it contains abundant lattice distortions that propagate vertically from one layer to another, leading to few-atoms-wide amorphous regions with weaker dielectric strength (see Figure S1, Supporting Information).<sup>[5,6]</sup> When integrated as dielectric in a device, the presence of these defective regions decreases the

homogeneity of the leakage current (see Figure S2a, Supporting Information), and reduces the lifetime of the device due to the stochastic nature of the dielectric breakdown (DB) process.<sup>[7]</sup> Moreover, the dielectric constant of h-BN is only  $\approx 3.9$ , which in ultra-scaled devices results in high leakage current and premature DB.<sup>[8,9]</sup> Furthermore, the synthesis of high-quality layered h-BN by CVD requires high temperatures  $>900$  °C,<sup>[10,11]</sup> which impedes its direct growth on patterned wafers. Consequently, finding insulating materials with a high dielectric constant that are compatible with graphene and other 2D materials is of paramount importance for the construction of advanced solid-state 2D materials based electronic devices and circuits.


CaF<sub>2</sub> is a dielectric material with a band gap of  $\approx 12.1$  eV and a dielectric constant of  $\approx 8.4$  that can be grown on a large-scale at low temperatures ( $\approx 250$  °C) using molecular beam epitaxy (MBE).<sup>[12]</sup> Thick ( $>100$  nm) stacks of CaF<sub>2</sub> have been used for more than 30 years in optoelectronics to fabricate windows, lenses, and lasers (among others) due to their excellent chemical stability when exposed to moisture and high relative humidities.<sup>[13]</sup> A recent report has demonstrated the use of ultra-thin ( $\approx 2$  nm) CaF<sub>2</sub> (111) films as gate dielectric in field-effect transistors (FETs) with bilayer molybdenum disulfide (MoS<sub>2</sub>) channels, and presented high on/off current ratios up to 10<sup>7</sup> and small hysteresis.<sup>[14]</sup> As the surface of the CaF<sub>2</sub> (111) film is terminated with inert fluorine atoms, this material does not present dangling bonds and it can form a van der Waals

C. Wen, Dr. F. Hui, Prof. M. Lanza  
Institute of Functional Nano & Soft Materials  
Collaborative Innovation Center of Suzhou Nano Science & Technology  
Soochow University  
199 Ren-Ai Road, Suzhou 215123, China  
E-mail: mlanza@suda.edu.cn

Dr. A. G. Bانشchikov, Dr. Y. Y. Illarionov, Prof. N. S. Sokolov  
Ioffe Institute  
Polytechnicheskaya 26, Saint Petersburg 194021, Russia

Dr. Y. Y. Illarionov, T. Knobloch, Prof. T. Grasser  
Institute for Microelectronics (TU Wien)  
Gusshausstrasse 27-29, Vienna 1040, Austria

Prof. W. Frammelsberger  
Department of Mechanical Engineering and Mechatronics  
Deggendorf Institute of Technology  
Dieter-Görlitz-Platz 1, Deggendorf 94469, Germany

 The ORCID identification number(s) for the author(s) of this article can be found under <https://doi.org/10.1002/adma.202002525>.

DOI: 10.1002/adma.202002525

interface with adjacent 2D layered materials,<sup>[13]</sup> making it one of the most promising dielectrics for future 2D materials based electronic devices and circuits. However, the density and type of defects in ultrathin CaF<sub>2</sub> films, as well as their effect on the dielectric performance of this material have never been analyzed in depth. In this investigation, we use characterization tools with sub-nanometer resolution to analyze the crystallographic structure, types of defects, and electrical properties of ultrathin CaF<sub>2</sub> films, and demonstrate that this material exhibits very high homogeneity, ultralow leakage current, and high dielectric strength. These observations are related to the absence of amorphous defective paths across the ultrathin CaF<sub>2</sub> film, as its cubic crystalline structure is continuous over long areas, something that so far has never been achieved in 2D layered dielectrics like multilayer h-BN.

High-quality ultrathin CaF<sub>2</sub> films were grown on a Si (111) surface by MBE at 250 °C (see Experimental Section). We collected >56 consecutive cross-sectional high-resolution transmission electron microscopy (TEM) images with sub-nanometer resolution, and at some locations also conducted energy-dispersive X-ray spectroscopy (EDX) as well as electron energy loss spectroscopy (EELS) to analyze the local chemical composition (see Experimental Section). As **Figure 1** shows, the cubic crystalline structure of the CaF<sub>2</sub> film follows different patterns in the TEM images, including 2D layered pattern with an

interlayer distance of  $\approx 0.32$  nm (Figure 1d), hexagonal pattern (Figure 1e), cubic pattern (Figure 1f), and point-like pattern (Figure 1g). This observation is related to the angle of the different orientations of the cubic CaF<sub>2</sub> crystal with respect to the electron beam of the TEM (see Figure S3, Supporting Information). More importantly, these patterns merge into one another very smoothly and without any visible defect (see Figure 1a–c and Figure S4, Supporting Information). This observation is fundamentally different to what has been often reported for CVD grown multilayer h-BN, which shows a layered structure with abundant few-atoms-wide amorphous regions embedded every < 10 nm (see Figures S1 and S2, Supporting Information).<sup>[5]</sup> In contrast, for ultrathin CaF<sub>2</sub> films we never observed amorphous defective regions similar to those observed in multilayer h-BN. The high-resolution TEM images also reveal that the thickness of the CaF<sub>2</sub> film is  $\approx 2.5$  nm, and that it shows minimal thickness fluctuations (<0.32 nm). This observation is further confirmed by topographic maps collected via atomic force microscopy (AFM), which shows that the surface of the CaF<sub>2</sub> sample is atomically flat (see Figure S5, Supporting Information), with a root mean square (RMS) roughness of only 54 pm, similar to that of industrial Si wafers.<sup>[15]</sup>

The correct chemical composition of the samples was confirmed by analyzing the concentration of Ca, F, and Si at multiple locations of the sample using EDX and EELS (see Figures S6

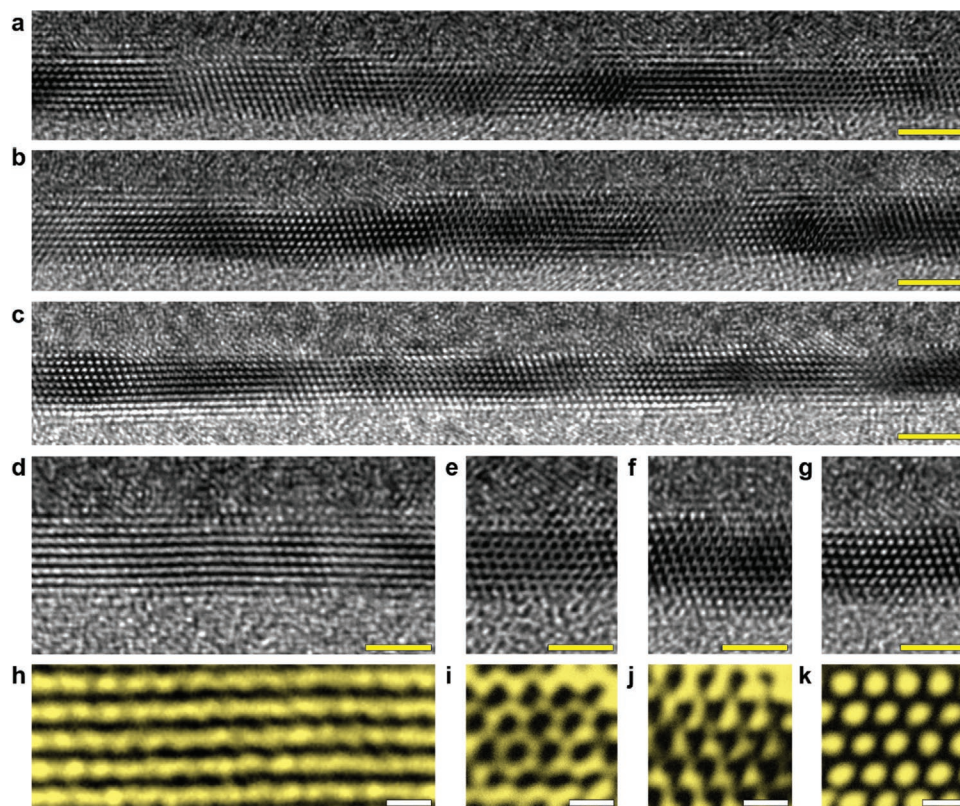


**Figure 1.** Cross-sectional high-resolution TEM images of ultrathin CaF<sub>2</sub> films. a–c) Large-area TEM images with sub-nanometer resolution showing the continuous cubic crystalline structure free of amorphous defective regions. The transition between them is very smooth (see Figure S4, Supporting Information), indicating that the CaF<sub>2</sub> crystal is continuous. d–g) Zoomed images showing the different crystallographic orientations detected, which are related to the angle of the different CaF<sub>2</sub> sub-lattices with respect to the electron beam of the TEM. h–k) Zoomed and false-colored images of (d)–(g) highlighting the type of crystallographic orientation. Scale bars: 3 nm in (a)–(c), 2 nm in (d)–(g), and 0.5 nm in (h)–(k).



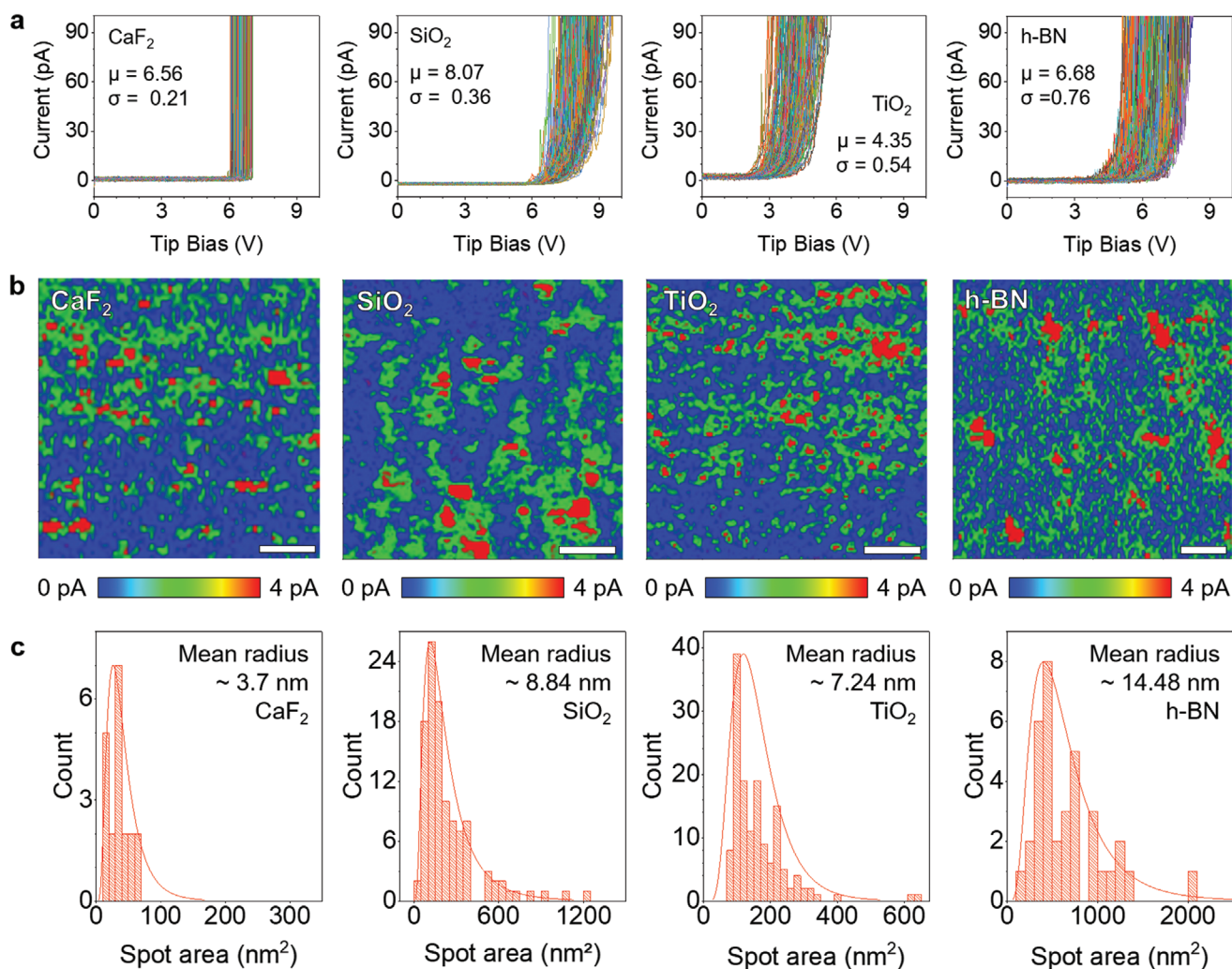


**Figure 2.** Nanoscale electrical homogeneity of CaF<sub>2</sub>, SiO<sub>2</sub>, TiO<sub>2</sub>, and h-BN observed via CAFM. a)  $I$ - $V$  curves collected on the surface of  $\approx 2.5$  nm CaF<sub>2</sub>, 4.7 nm SiO<sub>2</sub>, 2 nm TiO<sub>2</sub>/1.5 nm SiO<sub>x</sub>, and  $\approx 6$  nm h-BN by applying RVS from 0 to 10 V. Each plot shows  $> 300$   $I$ - $V$  curves collected at different locations. The mean value ( $\mu$ ) and standard deviation ( $\sigma$ ) of  $V_{\text{ON}}$  is indicated. b) Current maps collected on each sample by applying the minimum voltage needed to observe current above the noise level, which was 7 V for CaF<sub>2</sub>, 8.5 V for SiO<sub>2</sub>, 1.5 V for TiO<sub>2</sub>, and 5 V for h-BN. Scale bars in (b), 30 nm for CaF<sub>2</sub> and 100 nm for SiO<sub>2</sub>, TiO<sub>2</sub>, and h-BN. c) Statistical analysis of the size of the conductive spots observed in each map of panel (b).

and S7, Supporting Information); the concentration of parasitic elements like Cr (from the protective coating) and O (from the environment) was also mapped. Both tests clearly showed that the Ca and F signals overlap, and that they are sandwiched by Cr and Si. The O and Cr signals overlap due to the partial oxidation of the Cr film during the sputtering process, as expected.<sup>[16]</sup>

The electrical properties of the ultrathin CaF<sub>2</sub> films have been characterized at the nanoscale using a conductive atomic force microscope (CAFM) working in high-vacuum ( $\approx 10^{-6}$  Torr) and provided with solid Pt tips. Ramped voltage stresses (RVS) have been collected at  $> 280$  different randomly selected locations of the CaF<sub>2</sub> sample (see Experimental Section and Figure S8, Supporting Information), and the results have been compared to those obtained on industrial SiO<sub>2</sub> ( $\approx 4.7$  nm thick) grown by thermal oxidation on n<sup>+</sup>Si,  $\approx 2$  nm TiO<sub>2</sub> grown by atomic layer deposition (ALD) on 1.5 nm SiO<sub>x</sub>/n<sup>+</sup>Si (native silicon oxide), and  $\approx 6$  nm h-BN synthesized by CVD. It is important to highlight that all these samples are of premium quality, as confirmed

statistically via cross-sectional TEM and AFM (see Experimental Section and Figure S9, Supporting Information). As Figure 2a shows, the shape of the current versus voltage ( $I$ - $V$ ) curves collected on CaF<sub>2</sub> are radically different to those measured on all other dielectrics independently on the type of structure, i.e., 3D like SiO<sub>2</sub> and TiO<sub>2</sub> or 2D layered like h-BN. CaF<sub>2</sub> shows the lowest variability from one location to another, indicating that the CaF<sub>2</sub> sample is by far the most homogeneous. The homogeneity of the samples has been quantified by calculating the dispersion of the onset voltage ( $V_{\text{ON}}$ ), which is defined as the voltage at which the current starts to rapidly increase above 100 pA. The value of  $V_{\text{ON}}$  in CaF<sub>2</sub> is  $6.56 \pm 0.21$  V, compared to SiO<sub>2</sub> with  $8.07 \pm 0.36$  V, TiO<sub>2</sub> with  $4.35 \pm 0.54$  V, and CVD-grown h-BN with  $6.68 \pm 0.76$  V. This observation has been further confirmed by collecting current maps under a constant voltage at different locations of all the samples. As Figure 2b shows, for all the samples some locations (red spots) show higher currents than others, but in CaF<sub>2</sub> the size of the conductive (weak)

spots detected was always the smallest. More specifically, the mean radius of the weak spots in  $\text{CaF}_2$  is only  $\approx 3.7$  nm, which is remarkably smaller than in  $\text{SiO}_2$  ( $\approx 8.87$  nm),  $\text{TiO}_2$  ( $\approx 7.24$  nm), and h-BN ( $\approx 14.48$  nm), as shown in Figure 2c. See additional explanations in Note S1 (Supporting Information).

Another important observation in Figure 2a is that the value of  $V_{\text{ON}}$  for the  $I$ - $V$  curves collected on  $\approx 2.5$  nm  $\text{CaF}_2$  is close to that of the  $I$ - $V$  curves collected on  $\approx 4.7$  nm  $\text{SiO}_2$  and  $\approx 6$  nm h-BN, and much higher than that observed on  $\approx 3.5$  nm  $\text{TiO}_2/\text{SiO}_x$ , which is clear evidence that  $\text{CaF}_2$  can block the leakage current much more effectively than all the other materials. When the same experiments were repeated on  $\approx 2$  nm  $\text{SiO}_2$  grown by thermal oxidation on p-type Si (see Figure S10, Supporting Information),  $V_{\text{ON}}$  dramatically decreased down to  $2.31 \pm 0.25$  V, further evidencing the high ability of the ultrathin  $\text{CaF}_2$  ionic crystals to block leakage currents. Additional discussions are provided in Note S2 (Supporting Information).

Furthermore, the  $I$ - $V$  curves collected on  $\text{CaF}_2$  show an unusually steep current increase (see also Figure S11, Supporting Information), which is very different to that observed in all other materials. While in  $\text{SiO}_2$ ,  $\text{TiO}_2$ , and h-BN the shape of the  $I$ - $V$  curves fits well the conventional direct tunneling or Fowler–Nordheim tunneling conduction mechanisms (see Figure S12, Supporting Information), the  $I$ - $V$  curves collected in  $\text{CaF}_2$  do not fit any known form of leakage current, and the steep current increase seems to be more similar to the DB event. This behavior has been further analyzed by repeating the experiments using a logarithmic current-to-voltage preamplifier connected to the CAFM tip, which allows measuring currents in a very wide dynamic range from 10 pA to 1 mA.<sup>[17,18]</sup> As Figure 3 shows, all the  $I$ - $V$  curves collected in  $\text{SiO}_2$  exhibit leakage current followed by a sharp current increase that triggers the DB event. However, none of the  $I$ - $V$  curves collected in  $\text{CaF}_2$  exhibit this behavior. For  $\text{CaF}_2$  all the locations show a sudden current increase from sub-noise level to currents  $> 1$   $\mu\text{A}$ . In order to analyze if these currents correspond to the DB event, we have collected  $I$ - $V$  curves using current limitations (CLs) of 1 nA, 10 nA, 100 nA, and 1  $\mu\text{A}$ . As Figure S13 (Supporting Information) shows, when small CLs are applied (1 and 10 nA) the backward  $I$ - $V$  curves go back to the noise level before the voltage goes back to zero, meaning that the DB event was not completely triggered (although partial  $\text{CaF}_2$  degradation is obvious because the forward and backward  $I$ - $V$  curves do not overlap). However, when larger CLs (100 nA and 1  $\mu\text{A}$ ) are applied, the backward  $I$ - $V$  curves show an increase of current at low voltages, indicating that the DB has been effectively triggered—one should note that the current density ( $J$ ) across the tip/sample junction for CL = 100 nA is  $\approx 10^5$  A  $\text{cm}^{-2}$ , considering a very conservative contact area of  $\approx 100$  nm<sup>2</sup> (which in vacuum should be even smaller).<sup>[19,20]</sup> Consequently, the initial steep current increase detected at  $6.56 \pm 0.21$  V corresponds to the DB event, and the current fluctuations detected after that are related to post-DB phenomena, such as avalanche currents,<sup>[21]</sup> electromigration,<sup>[22]</sup> and dielectric-breakdown-induced epitaxy<sup>[23]</sup> (DBIE). The latter effect has been further confirmed by stopping the RVS at 8 V, which triggers a clean DB without DBIE (see Figures S14 and S15, Supporting Information). These experiments demonstrate that the leakage current across ultrathin  $\text{CaF}_2$  before the DB is much smaller than in  $\text{SiO}_2$ ,  $\text{TiO}_2$ , and h-BN, as it cannot

be detected by the tip of the CAFM. This behavior, which has never been observed before in any other ultrathin dielectric, is a very important property that can be exploited to improve the reliability and time-dependent variability of electronic devices.

In addition, from Figure 3 the dielectric strength of both  $\text{CaF}_2$  and  $\text{SiO}_2$  can be calculated dividing the DB voltage by the thickness of each insulating material, resulting in values of  $\approx 27.8 \pm 1.7$  MV  $\text{cm}^{-1}$  and  $20.3 \pm 0.9$  MV  $\text{cm}^{-1}$ . It is worth noting that the dielectric strength of the  $\text{SiO}_2$  sample is consistent with that previously observed in other industrial  $\text{SiO}_2$  samples,<sup>[24]</sup> indicating the high quality of the thermal  $\text{SiO}_2$  and the validity of the characterization method employed. Note that this value is higher than those previously reported for  $\text{TiO}_2$  ( $\approx 3$  MV  $\text{cm}^{-1}$ )<sup>[25]</sup> and mechanically exfoliated h-BN ( $\approx 12.0$  MV  $\text{cm}^{-1}$ ) via CAFM.<sup>[26–28]</sup> Additional discussion about the calculation and meaning of dielectric strength can be found in Note S3 (Supporting Information). This observation further indicates the extraordinary potential of ultrathin  $\text{CaF}_2$  films to serve as dielectric in nanoelectronic devices.

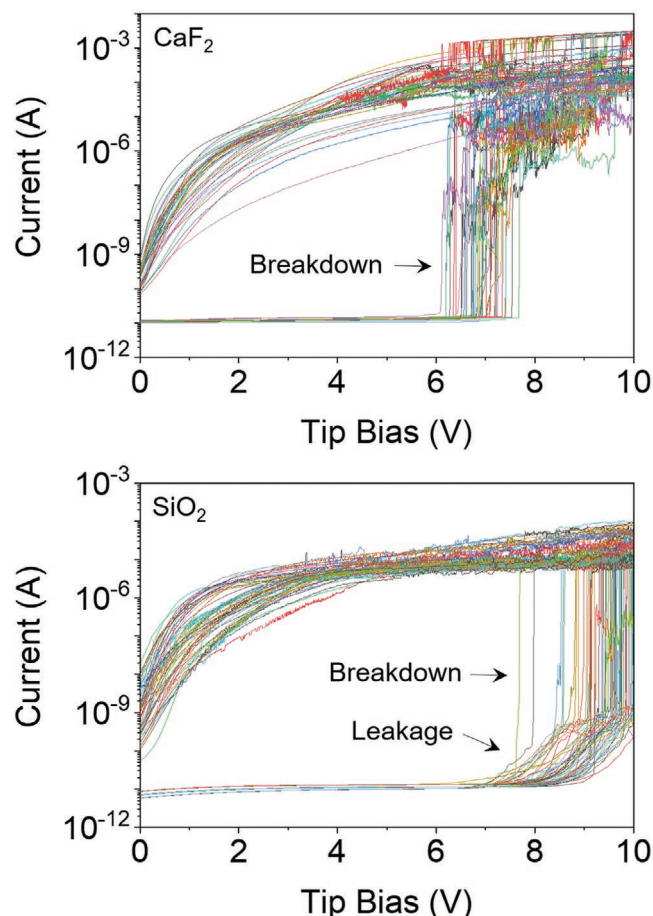


**Figure 3.** Analysis of leakage current and dielectric strength in  $\text{CaF}_2$  and  $\text{SiO}_2$ .  $I$ - $V$  curves collected on the surface of  $\approx 2.5$  nm  $\text{CaF}_2$  and  $\approx 4.7$  nm  $\text{SiO}_2$  samples by applying RVS from 0 to 10 V, using a logarithmic current-to-voltage preamplifier. For  $\text{CaF}_2$  and  $\text{SiO}_2$  a total of 43 and 58 locations have been analyzed. The dielectric strength of  $\text{CaF}_2$  is  $27.8 \pm 1.7$  MV  $\text{cm}^{-1}$ , and the dielectric strength of  $\text{SiO}_2$  is  $20.3 \pm 0.9$  MV  $\text{cm}^{-1}$ . The leakage current across of the  $\text{CaF}_2$  film is so low that it cannot be detected with the CAFM.

Future studies on CaF<sub>2</sub> dielectrics should include the characterization of other intrinsic dielectric properties, such as capacitance, dielectric constant, and time and frequency-dependent stability. Furthermore, the synthesis of high-quality CaF<sub>2</sub> on other substrates different than Si (111) may be necessary in order to facilitate its integration on 2D materials based solid-state electronic devices. Finally, carrying out electrical reliability analyses on test structures with areas similar to that of the channel of state-of-the-art FETs would be very useful to further understand the performance of CaF<sub>2</sub> at the device level. We are aware that developing such studies in a statistical and reliable manner would require a substantial amount of work that would deserve one/few independent publication/s, and for that reason such tasks are out of the scope here.

In conclusion, we have demonstrated that ultrathin ( $\approx 2.5$  nm) CaF<sub>2</sub> films show outstanding performance as dielectric when exposed to electrical stresses. By applying RVS with the tip of a CAFM at multiple locations, we have statistically demonstrated that CaF<sub>2</sub> is more homogeneous and has a higher dielectric strength ( $\approx 27.8$  MV cm<sup>-1</sup>) than SiO<sub>2</sub> ( $\approx 20.3$  MV cm<sup>-1</sup>), TiO<sub>2</sub> ( $\approx 3$  MV cm<sup>-1</sup>) and h-BN ( $\approx 12.0$  MV cm<sup>-1</sup>), and that the leakage current across CaF<sub>2</sub> is orders of magnitude smaller than in nearly twice as thick SiO<sub>2</sub>. Cross-sectional high-resolution TEM images demonstrate that the main reason behind this enhanced dielectric performance is that the cubic crystalline structure of the ultrathin CaF<sub>2</sub> film is continuous and defect-free over large regions, which prevents the formation of electrically weak spots.

## Experimental Section

**Calcium Fluoride Growth:** Ultrathin CaF<sub>2</sub> layers were grown by MBE on weakly doped single-crystal n-Si (111) substrates with  $N_D = 10^{15}$  cm<sup>-3</sup> and a misorientation of 5–10 angular min. Before the growth process, a protective oxide layer was formed after chemical treatment.<sup>[29]</sup> This layer was removed by annealing for 2 min at 1200 °C under ultrahigh-vacuum conditions ( $10^{-8}$ – $10^{-7}$  Pa). This allowed to obtain an atomically clean  $7 \times 7$  Si (111) surface. The CaF<sub>2</sub> film was grown on this surface by MBE at 250 °C, which is known to be the optimum temperature to produce pinhole-free homogeneous CaF<sub>2</sub> layers.<sup>[30]</sup> The deposition rate of CaF<sub>2</sub> measured by a quartz oscillator was  $\approx 1.3$  nm min<sup>-1</sup>. The growth processes and crystalline quality of the CaF<sub>2</sub> layers were monitored using reflection high-energy electron diffraction, with an electron energy of 15 keV.

**Preparation of the SiO<sub>2</sub>, TiO<sub>2</sub> and h-BN Samples:** The ultrathin SiO<sub>2</sub> films with a thickness of  $\approx 4.7$  nm were grown by thermal oxidation of n<sup>+</sup>Si (1 0 0) wafers with a resistivity of 0.002–0.003  $\Omega$  cm at the laboratories of Infineon Technologies. Note that this company has been growing SiO<sub>2</sub> of outstanding quality (i.e., low amount of defects and ultraflat surface) for more than 30 years. The  $\approx 2$  nm TiO<sub>2</sub> films were grown on n-type Si wafers, with a resistivity ranging between 0.008 and 0.02  $\Omega$  cm, using a plasma-enhanced ALD system from Cambridge Nanotech. These wafers had a 1.5 nm native oxide on top, leading to a  $\approx 2$  nm TiO<sub>2</sub>/1.5 nm SiO<sub>x</sub>/n<sup>+</sup>Si structure. The Ti and O sources used were tetrakis(dimethyl amido) titanium (Ti(NMe<sub>2</sub>)<sub>4</sub>) and oxygen inductively coupled discharge, respectively. The exposure time to Ti(NMe<sub>2</sub>)<sub>4</sub> during one ALD cycle was 0.1 s, and the interval time between two exposures was 10 s, resulting in a growth rate of 0.51 Å per cycle. The  $\approx 6$  nm h-BN samples were grown by CVD on Cu substrates at 1000 °C using ammonia borane as precursor.<sup>[6]</sup> The quality of these samples represented state-of-the-art, as confirmed by the low amount of defects detected via TEM and the minimal thickness fluctuations proved by AFM. The  $\approx 2$  nm SiO<sub>2</sub> grown by thermal oxidation on p-type Si (with  $N_A = 5 \times 10^{15}$  cm<sup>-3</sup>), used only in

Figure S10 (Supporting Information), was also grown at the laboratories of Infineon Technologies.

**Cross-Sectional High-Resolution TEM Characterization:** In order to protect the samples and provide a good contrast in the TEM image, 15 nm Cr was sputtered on the samples using a Gatan 682 precision etching and coating system (PECS). Then, 2  $\mu$ m long thin lamellas were cut with a focus ion beam from FEI (model: Helios Nanolab 450S) with a power of 30 kV and current of 7.7 pA. After that, the lamellas were placed on a copper grid and scanned with a high-resolution TEM (TITAN Themis 200, FEI) in high vacuum ( $10^{-6}$  Pa). The chemical composition of the samples was analyzed by EDX (model: Bruker super-EDS) and EELS (model: Gatan) tools integrated in the TEM. For each sample, >56 high-resolution TEM images at different locations were collected, and small differences from one location to another were observed.

**Nanoscale Topographic and Electrical Characterization:** The surface roughness and conductivity of all the samples were characterized at the nanoscale using a NX-HighVac CAFM from Park Systems working in high vacuum ( $10^{-6}$  Torr). In order to avoid tip degradation during the experiments, solid Pt AFM tips from Rocky Mountain Nanotechnology (model: RMN-25Pt300B) were used, which have a typical radius at their apex of  $\approx 20$  nm and a constant force of  $\approx 18$  N m<sup>-1</sup>. The measurements were carried out by applying a contact force of  $\approx 20$  nN, which ensures good electrical contact in vacuum and at the same time is enough low to avoid pressure effects.<sup>[31,32]</sup> All the samples were glued to the AFM sample holder using conductive silver paint. RVS were applied at different locations of the samples using the matrix tool integrated in the software of the CAFM (see Figure S8, Supporting Information). Each matrix of points measured was located >5 mm away from the previous one, leading to a large-area characterization. The topographic and current maps were collected in contact mode by applying the minimum voltage required to observe current above the noise level. The voltages, both in RVS and current maps, were applied to the CAFM tip (top electrode) while keeping the substrate (bottom electrode) grounded. The topographic maps aimed to evaluate the surface roughness were always collected without applying any bias.

## Supporting Information

Supporting Information is available from the Wiley Online Library or from the author.

## Acknowledgements

This work was supported by the Ministry of Science and Technology of China (grant no. BRICS2018-211-2DNEURO), the National Natural Science Foundation of China (grant nos. 11661131002, 61874075), the Ministry of Finance of China (grant no. SX21400213), the Russian Foundation for Basic Research (grant no. 18-57-80006 BRICS), the 111 Project from the State Administration of Foreign Experts Affairs of China, the Collaborative Innovation Centre of Suzhou Nano Science & Technology, the Jiangsu Key Laboratory for Carbon-Based Functional Materials & Devices, the Priority Academic Program Development of Jiangsu Higher Education Institutions, and the Austrian Science Foundation (grant no. I2606-N30). Dr. Rudolf Berger from Infineon Technologies is acknowledged for providing the SiO<sub>2</sub> samples. Mr. Michael Quell from TU Wien and Prof. Mikhail Vexler from the Ioffe Physical-Technical Institute are acknowledged for useful discussions related to the growth and structure of CaF<sub>2</sub>. Engineers from Park Systems are acknowledged for technical advice on the use of the NX-HighVac CAFM.

## Conflict of Interest

The authors declare no conflict of interest.



## Keywords

2D materials, calcium fluoride, dielectric strength, van der Waals interfaces

Received: April 13, 2020

Revised: June 8, 2020

Published online:

- 
- [1] K. Kang, S. Xie, L. Huang, Y. Han, P. Y. Huang, K. F. Mak, C.-J. Kim, D. Müller, J. Park, *Nature* **2015**, 520, 656.
- [2] Y. Y. Illarionov, G. Rzepa, M. Waltl, T. Knobloch, A. Grill, M. M. Furchi, T. Mueller, T. Grasser, *2D Mater.* **2016**, 3, 035004.
- [3] C. R. Dean, A. F. Young, I. Meric, C. Lee, L. Wang, S. Sorgenfrei, K. Watanabe, T. Taniguchi, P. Kim, K. L. Shepard, J. Hone, *Nat. Nanotechnol.* **2010**, 5, 722.
- [4] H. Pandey, M. Shaygan, S. Sawallich, S. Kataria, Z. Wang, A. Noculak, M. Otto, M. Nagel, R. Negra, D. Neumaier, M. C. Leme, *IEEE Trans. Electron Devices* **2018**, 65, 4129.
- [5] C. Pan, Y. Ji, N. Xiao, F. Hui, K. Tang, Y. Guo, X. Xie, F. M. Puglisi, L. Larcher, E. Miranda, L. Jiang, Y. Shi, I. Valov, P. C. McIntyre, R. Waser, M. Lanza, *Adv. Funct. Mater.* **2017**, 27, 1604811.
- [6] Y. Shi, X. Liang, B. Yuan, V. Chen, H. Li, F. Hui, Z. Yu, F. Yuan, E. Pop, H.-S. P. Wong, M. Lanza, *Nat. Electron.* **2018**, 1, 458.
- [7] F. Palumbo, C. Wen, S. Lombardo, S. Pazos, F. Aguirre, M. Eizenberg, F. Hui, M. Lanza, *Adv. Funct. Mater.* **2019**, 11, 1900657.
- [8] R. Geick, C. H. Perry, G. Rupprecht, *Phys. Rev.* **1966**, 146, 543.
- [9] N. Guo, J. Wei, Y. Jia, H. Sun, Y. Wang, K. Zhao, X. Shi, L. Zhang, X. Li, A. Cao, H. Zhu, K. Wang, D. Wu, *Nano Res.* **2013**, 6, 602.
- [10] K. K. Kim, A. Hsu, X. Jia, S. M. Kim, Y. Shi, M. Dresselhaus, T. Palacios, J. Kong, *ACS Nano* **2012**, 6, 8583.
- [11] J. S. Lee, S. H. Choi, S. J. Yun, Y. I. Kim, S. Boandoh, J.-H. Park, B. G. Shin, H. Ko, S. H. Lee, Y.-M. Kim, Y. H. Lee, K. K. Kim, S. M. Kim, *Science* **2018**, 362, 817.
- [12] R. C. Ropp, *Encyclopedia of the Alkaline Earth Compounds*, Elsevier, Amsterdam, The Netherlands **2013**, Ch. 2.
- [13] A. Koma, K. Saiki, Y. Sato, *Appl. Surf. Sci.* **1990**, 41, 451.
- [14] Y. Y. Illarionov, A. G. Banskchikov, D. K. Polyushkin, S. Wachter, T. Knobloch, M. Thesberg, L. Mennel, M. Paur, M. Stöger-Pollach, A. Steiger-Thirnsfeld, M. I. Vexler, M. Waltl, N. S. Sokolov, T. Mueller, T. Grasser, *Nat. Electron.* **2019**, 2, 230.
- [15] G. D. Wilk, Y. Wei, R. M. Wallace, (Texas Instruments Inc), *US* **6,020,247**, **2010**.
- [16] B. Navinšek, P. Panjan, *Surf. Coat. Technol.* **1993**, 59, 244.
- [17] L. Aguilera, M. Lanza, A. Bayerl, M. Porti, M. Nafria, X. Aymerich, *J. Vac. Sci. Technol., B* **2009**, 27, 360.
- [18] F. Hui, M. Lanza, *Nat. Electron.* **2019**, 2, 221.
- [19] W. Frammelsberger, G. Benstettera, J. Kiely, R. Stamp, *Appl. Surf. Sci.* **2007**, 253, 3615.
- [20] M. Lanza, M. Porti, M. Nafria, X. Aymerich, E. Whittaker, B. Hamilton, *Rev. Sci. Instrum.* **2010**, 81, 106110.
- [21] G. Gradinaru, T. S. Sudarshan, *J. Appl. Phys.* **1993**, 73, 7643.
- [22] T. Frank, S. Moreau, C. Chappaz, P. Leduc, L. Arnaud, A. Thuair, E. Chery, F. Lorut, L. Anghel, G. Poupon, *Microelectron. Reliab.* **2013**, 53, 17.
- [23] C. H. Tung, K. L. Pey, L. J. Tang, M. K. Radhakrishnan, W. H. Lin, F. Palumbo, S. Lombardo, *Appl. Phys. Lett.* **2003**, 83, 2223.
- [24] E. Y. Wu, *IEEE Trans. Electron Devices* **2019**, 66, 4523.
- [25] J. Y.-M. Lee, B. C. Lai, in *Handbook of Thin Films Materials*, Vol. 3 (Ed: H. S. Nalwa), Academic Press, Cambridge, MA, USA **2002**.
- [26] Y. Ji, C. Pan, M. Zhang, S. Long, X. Lian, F. Miao, F. Hui, Y. Shi, L. Larcher, E. Wu, M. Lanza, *Appl. Phys. Lett.* **2016**, 108, 012905.
- [27] Y. Hattori, T. Taniguchi, K. Watanabe, K. Nagashio, *Appl. Phys. Lett.* **2016**, 109, 253111.
- [28] Y. Hattori, T. Taniguchi, K. Watanabe, K. Nagashio, *ACS Nano* **2015**, 9, 916.
- [29] A. Ishizaka, Y. Shiraki, *J. Electrochem. Soc.* **1986**, 133, 666.
- [30] Y. Y. Illarionov, M. I. Vexler, V. V. Fedorov, S. M. Sutturin, N. S. Sokolov, *J. Appl. Phys.* **2014**, 115, 223706.
- [31] A. Ranjan, N. Raghavan, J. Molina, S. J. O'Shea, K. Shubhakar, K. L. Pey, *Microelectron. Reliab.* **2016**, 64, 172.
- [32] S. Chen, L. Jiang, M. Buckwell, X. Jing, Y. Ji, E. Grustan-Gutierrez, F. Hui, Y. Shi, M. Rommel, A. Paskaleva, G. Benstetter, W. H. Ng, A. Mehon, A. J. Kenyon, M. Lanza, *Adv. Funct. Mater.* **2018**, 28, 1802266.